SUPPLEMENTARY MATERIAL

The AFM micrographs of 14, 16, and 18 nm of BiSb are shown in Fig. S1 (a)-(f). It is evident that when the thickness of BiSb increased beyond 14 nm, individual island growth of BiSb increased, which changed the morphology from a uniform grain structure of BiSb to a nonuniform island growth. The reason for such a 3D island growth after the critical thickness of 14 nm, is the high surface energy of BiSb. This mechanism can be understood from the AFM images shown below. To minimize the surface energy, BiSb forms as 3D islands. Along with this, Bi and Sb atoms have high surface diffusivities, which force them to coalesce into islands as the film thickness increases. The height of the island increases from ~ 16 nm in the case of BiSb (14 nm) to 26 nm in BiSb (18 nm). Tou et al. have reported that the roughness of BiSb increases with thickness due to the island growth, as observed from our AFM results compared with the layer thickness.[1] We have added the AFM micrographs of the BiSb (14, 16, 18 nm) films to support our claims that the roughness of the BiSb films increases after 14 nm.

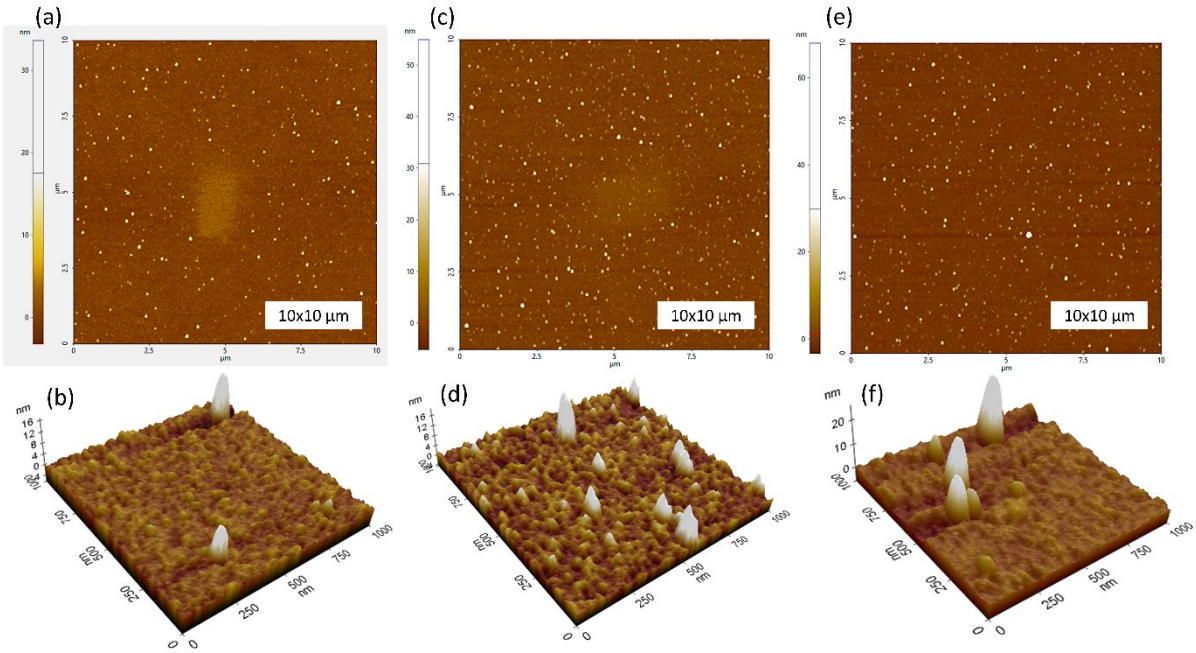

Fig. S1. AFM micrographs and the 3D images showing islands in (a), (b) Si/BiSb (14 nm); (c), (d) Si/BiSb (16 nm), and (e), (f) Si/BiSb (18 nm)

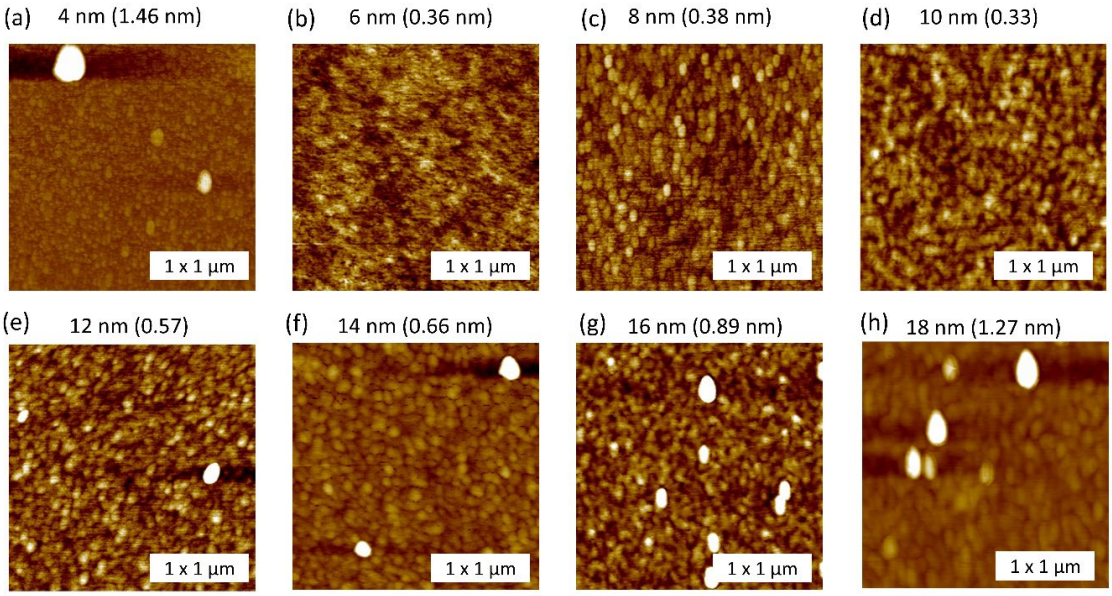

Fig. S2. AFM micrographs and the Ra values of (a) BiSb (4 nm), (b) BiSb (6 nm), (a) BiSb (8 nm), (d) BiSb (10 nm), (e) BiSb (12 nm), (f) BiSb (14 nm), (g) BiSb (16 nm), (h) BiSb (18 nm)

The AFM micrographs (1 × 1 µm) of all the samples (BiSb (4nm) to BiSb (18 nm) at 2 nm intervals) along with the Ra values are shown in Fig. S2 (a) to (h). The roughness (Ra) values vs the thickness of BiSb (4, 5, 6, 8, 10, 12, 14, 16, and 18 nm) are shown in Fig. S3.

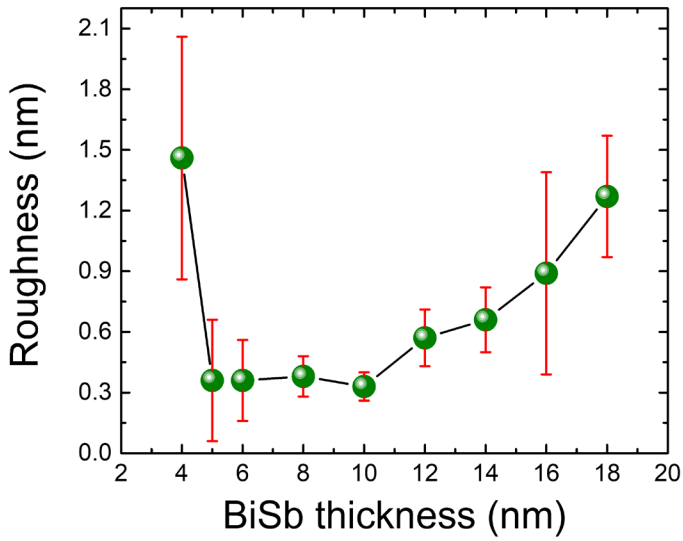

Fig. S3. Roughness vs thickness of BiSb (4, 5, 6, 8, 10, 12, 14, 16, and 18 nm)

Magnetic field angular dependence of V_{sym} for the samples A1, A2, A4, B1 and B2 are shown in the Fig. S4.

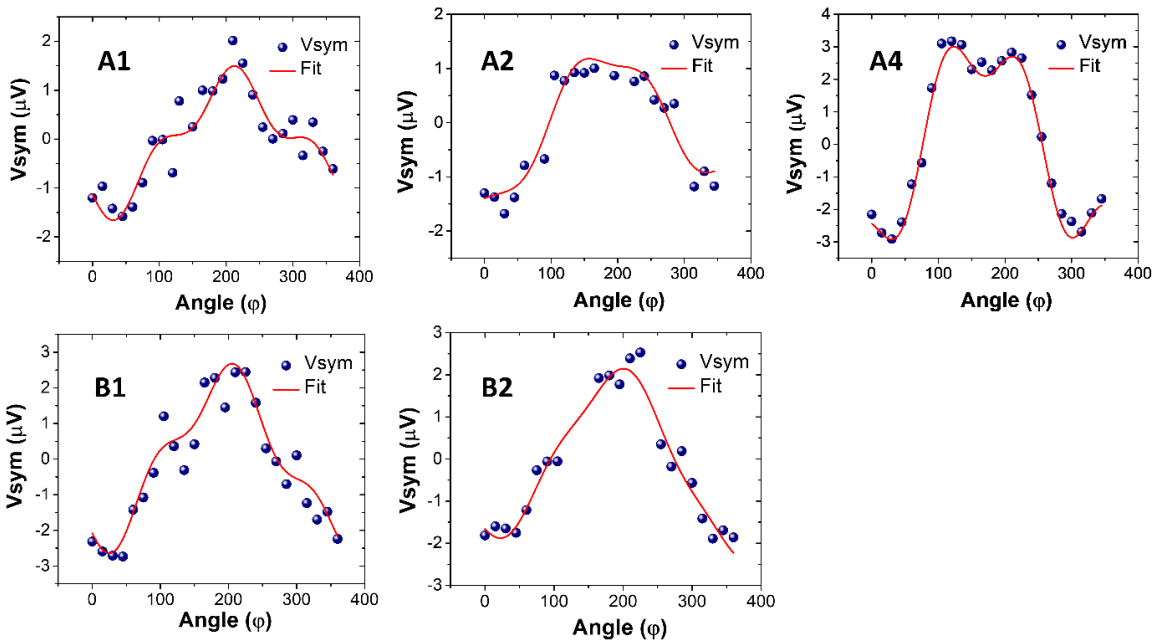

Fig. S4. V_{sym} data of samples A1, A2, A4, B1, and B2 measured at the field in 360 degrees in the in-plane direction, and the solid line is the fit to equation (3)

The change in the damping parameter and the spin mixing conductance are the parameters that decide J_s. They both qualitatively give an idea of the spin current that is generated and pumped by Py into the adjacent layers. Since the thickness of Py is constant in all the samples, it is expected that the amount of spin current generated from Py is constant. Thereby, the J_s values are similar in all the samples except where there is no space layer, i.e, Ti (0). The improvement in the ξ when the Ti is increased from 0 to 3 can be understood as the effectiveness of the Ti as a diffusion barrier. As we mentioned in the manuscript, though the SOC of the inter-layer Ti is smaller, spins tend to relax from their initial state when they travel for longer distances in Ti. However, when the thickness of Ti is high (4 and 8 nm) there will be a slight reduction in the actual spin current that is reaching BiSb due to the scattering in Ti. This is the reason why there is a reduction in the ξ when the thickness of Ti increases beyond 4 nm as shown in Fig. S5 (a).

Fig. S5(b) shows the comparison of ξ and spin current density, which are estimated from the ISHE experiments. In ISHE experiments, the source of spin current is the ferromagnetic layer, i.e., Py in our case. In the samples shown in Fig. S5(b), the thickness of Py and Ti are constant. Since the thickness of Py is constant, we expect that the quantity of spin current remains constant in all three samples, thereby similar spin current density in all samples. The change in ξ is due to the spin-to-charge conversion in BiSb with different thicknesses because, with increasing thickness of BiSb, the TSS becomes stable, as shown in work by Han et al.[1]

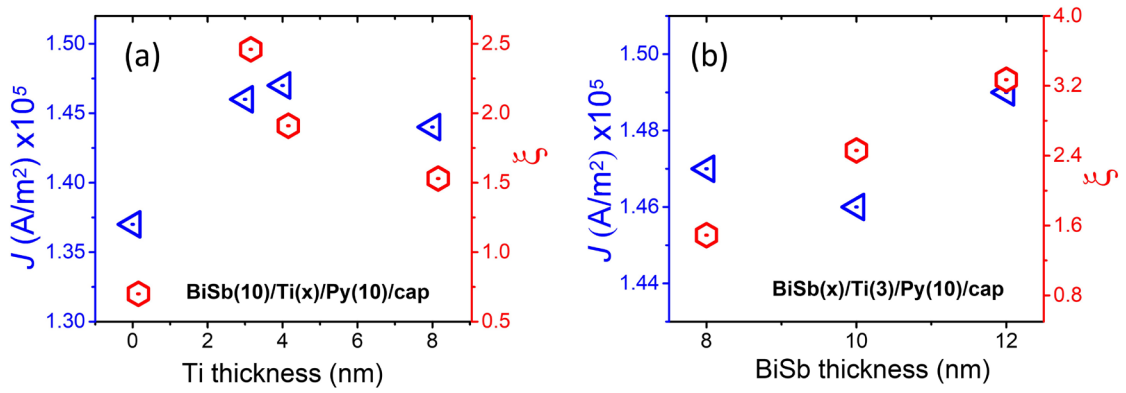

Fig. S5. (a) Ti thickness dependence of spin current density (J) and the spin Hall angle (ξ) in BiSb(10)/Ti(x)/Py(10)/cap stacks, (b) BiSb thickness dependence of spin current density (J) and the spin Hall angle in BiSb(x)/Ti(3)/Py(10)/cap stacks

The dependence of symmetric (S) and asymmetric (A) components of the voltage on the in-plane angular magnetic field for the samples A2, A3 and A4 are shown in the Fig. S6.

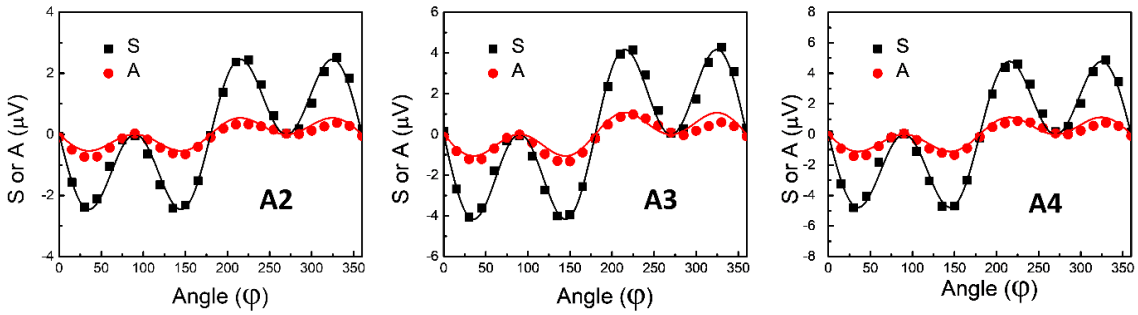

Fig. S6. Angular magnetic field (in-plane) dependence of Symmetric (S) and Asymmetric (A) components of the voltage for the samples A2, A3 and A4

The crystallite/grain size of the BiSb films with thicknesses of 8, 10, 12, and 18 nm is estimated from the (003) orientation in XRD patterns using the Scherrer formula. The values are listed below in the table.

Table S1: The grain size estimated using (003) orientation in BiSb films of thicknesses 8, 10, 12, 18 nm

Sample	**2θ (deg.)**	**θ (deg.)**	**FWHM (deg.)**	**Crystallite size (nm)**
BiSb (8 nm)	22.57	11.28	1.02	7.87
BiSb (10 nm)	22.38	11.19	1.09	7.41
BiSb (12 nm)	22.68	11.34	0.88	9.17
BiSb (18 nm)	22.63	11.31	0.53	15.15

References

1. Fan, T., Huynh, N., Khang, D., Nakano, S. & Hai, P. N. Ultrahigh efficient spin orbit torque magnetization switching in fully sputtered topological insulator and ferromagnet multilayers. *Scientific Reports* 1–8 (2022) doi:10.1038/s41598-022-06779-3.

2. Barua, S. & Rajeev, K. P. Status of surface conduction in topological insulators. *AIP Advances* **4**, 017135 (2014).

3. Han, J. & Liu, L. Topological insulators for efficient spin–orbit torques. *APL Materials* **9**, 060901 (2021).